A SYSTEMATIC STUDY OF CARBON–OXYGEN WHITE DWARF MERGERS: MASS COMBINATIONS FOR TYPE Ia SUPERNOVAE

Yushi Sato[1,2], Naohito Nakasato[3], Ataru Tanikawa[3,4], Ken'ichi Nomoto[5,7], Keiichi Maeda[6,5], and Izumi Hachisu[2]

[1] Department of Astronomy, Graduate School of Science, The University of Tokyo, 7-3-1 Hongo, Bunkyo-ku, Tokyo 113-0033, Japan
[2] Department of Earth Science and Astronomy, College of Arts and Sciences, The University of Tokyo, 3-8-1 Komaba, Meguro-ku, Tokyo 153-8902, Japan; sato@ea.c.u-tokyo.ac.jp
[3] Department of Computer Science and Engineering, University of Aizu, Tsuruga Ikki-machi Aizu-Wakamatsu, Fukushima 965-8580, Japan
[4] RIKEN Advanced Institute for Computational Science, 7-1-26 Minatojima-minami-machi, Chuo-ku, Kobe, Hyogo 650-0047, Japan
[5] Kavli Institute for the Physics and Mathematics of the Universe (WPI), The University of Tokyo, 5-1-5 Kashiwanoha, Kashiwa, Chiba 277-8583, Japan
[6] Department of Astronomy, Kyoto University, Kitashirakawa-Oiwake-cho, Sakyo-ku, Kyoto 606-8502, Japan

ABSTRACT

Mergers of two carbon–oxygen (CO) white dwarfs (WDs) have been considered to be progenitors of Type Ia supernovae (SNe Ia). Based on smoothed particle hydrodynamics (SPH) simulations, previous studies have claimed that mergers of CO WDs lead to SN Ia explosions either in the dynamical merger phase or the stationary rotating merger remnant phase. However, the mass range of CO WDs that lead to SNe Ia has not yet been clearly identified. In the present work, we perform systematic SPH merger simulations for the WD masses ranging from $0.5\,M_\odot$ to $1.1\,M_\odot$ with higher resolutions than the previous systematic surveys and examine whether or not carbon burning occurs dynamically or quiescently in each phase. We further study the possibility of SNe Ia explosions and estimate the mass range of CO WDs that lead to SNe Ia. We found that when both WDs are massive, i.e., in the mass range of $0.9\,M_\odot \leqslant M_{1,2} \leqslant 1.1\,M_\odot$, they can explode as an SN Ia in the merger phase. On the other hand, when the more massive WD is in the range of $0.7\,M_\odot \leqslant M_1 \leqslant 0.9\,M_\odot$ and the total mass exceeds $1.38\,M_\odot$, they can finally explode in the stationary rotating merger remnant phase. We estimate the contribution of CO WD mergers to the entire SN Ia rate in our galaxy to be of $\lesssim 9\%$. Thus, it might be difficult to explain all galactic SNe Ia with CO WD mergers.

Key words: binaries: close – galaxies: evolution

1. INTRODUCTION

Type Ia supernovae (SNe Ia) play important roles in the determination of cosmological parameters as luminous standard candles (e.g., Riess et al. 1998; Perlmutter et al. 1999) and in the chemical evolution of galaxies as major sources of iron group elements (e.g., Kobayashi et al. 1998). However, their progenitors have still not yet been identified (e.g., Maoz et al. 2014). They are considered to be thermonuclear explosions of CO WDs in a binary system in which a WD accretes mass from its companion and the WD mass approaches the Chandrasekhar mass ($M_{Ch} \sim 1.4\,M_\odot$), but, whether the WD's companion is a non-degenerate star, i.e., a single degenerate (SD) model, or a degenerate star, i.e., a double degenerate (DD) model, is still a matter of debate. In the SD model, a CO WD accretes hydrogen-rich/helium-rich gas from its companion, thereby increasing its mass up to M_{Ch}. Carbon burning starts at the center of the CO WD and explodes as an SN Ia (Whelan & Iben 1973; Nomoto 1982; Hachisu et al. 1996, 1999a, 1999b). By contrast, in the DD model, both components are CO WDs. Because binaries lose their orbital angular momentum by emitting gravitational waves, they will eventually merge. If their total mass exceeds M_{Ch}, the binary finally explodes as an SN Ia (Iben & Tutukov 1984; Webbink 1984).

Some clues to the progenitors of SNe Ia have been found in recent observations. In particular, neither surviving companions nor signatures of them were detected in some SNe Ia (e.g., Schaefer & Pagnotta 2012). This fact supports the DD model, although no detection of companions can also be explained by the SD model (Di Stefano et al. 2011; Justhum 2011; Hachisu et al. 2012). In some SNe Ia, signatures of circumstellar matter were detected (e.g., Patat et al. 2007; Blondin et al. 2009; Simon et al. 2009; Sternberg et al. 2011). This supports the SD model (e.g., Maoz et al. 2014, for a recent review), although this can be explained by some DD models (Raskin & Kasen 2013; Shen et al. 2013; Soker et al. 2013). Observations have still not clarified which model is accurate for the main progenitors of SNe Ia, i.e., the SD model or the DD (or other type) model.

There are theoretical difficulties with the DD model as the progenitor model. Some theoretical studies have indicated that CO WD mergers cannot become SNe Ia, but instead collapse to neutron stars (e.g., Saio & Nomoto 1985, 2004; Nomoto & Kondo 1991). In these studies the authors calculated only the evolution of merger remnants after DD systems merged. Their calculations were one-dimensional (1D), spherically symmetric, and assumed a stationary state. However, the merger of a DD system is a three-dimensional (3D) and dynamic event, so multi-dimensional hydrodynamic simulations are necessary to reach a definite conclusion. Benz et al. (1990) used a 3D smoothed particle hydrodynamics (SPH) code and simulated mergers of two CO WDs. Following this work, there have been several studies of mergers of DD systems (Rasio & Shapiro 1995; Segretain et al. 1997; Guerrero et al. 2004; Yoon et al. 2007; Lorén-Aguilar et al. 2009; Fryer et al. 2010; Pakmor et al. 2010; Dan et al. 2011; Raskin et al. 2012, 2014; Moll et al. 2014). These authors concluded that some DD pairs can explode as SNe Ia. Such successful models can be divided by the dynamical phase when the SN Ia explosion occurs.

---

[7] Hamamatsu Professor.

Pakmor et al. ([2010]) simulated mergers of massive CO WDs ($\sim 0.9\,M_\odot$) and found that carbon detonation initiates during the dynamic merger phase because of the compressional heating by the disrupted secondary which violently accretes onto the primary. The binary system finally explodes as a subluminous SN Ia. Pakmor et al. ([2012a]) also simulated mergers of more massive CO WDs ($1.1 + 0.9\,M_\odot$) and found that such systems lead to normal SNe Ia.

If carbon detonation does not initiate in the dynamic merger phase, the remnant undergoes three other phases. The first phase is the early remnant phase (e.g., Shen et al. [2012]; Kashyap et al. [2015]), 100–1000 s after the secondary is completely disrupted. In this phase, the merger remnant has not yet reached a quasi-stationary state and still has small non-axisymmetric structures. The second phase is the viscous evolution phase (Schwab et al. [2012]; Shen et al. [2012]; Ji et al. [2013]), 10^4–10^8 s after merging. In this phase, the remnant reaches a quasi-stationary, axisymmetric state and it evolves in a viscous timescale. The third phase is the thermal evolution phase (Saio & Nomoto [1985], [2004]; Yoon et al. [2007]; Shen et al. [2012]), $\gtrsim 10^3$ years. If off-center carbon burning occurs in these three phases before the rotating core of the remnant reaches $M_{\rm Ch}$, it likely converts the CO WD to an oxygen–neon–magnesium (ONeMg) WD. The ONeMg WD finally collapses to a neutron star when its core mass reaches $M_{\rm Ch}$. Yoon et al. ([2007]) simulated a merger of CO WDs with masses of $0.9 + 0.6\,M_\odot$ and followed the evolution of the merger remnant. They found that the remnant can avoid off-center carbon burning and explodes as an SN Ia in the thermal evolution phase if it satisfies several conditions.

Thus, the authors of these works concluded that some DD systems can become SNe Ia. However, the mass range of CO WDs that lead to SNe Ia has not yet been clarified. In this work, we simulate mergers of CO WDs with a mass range of $0.5 - 1.1\,M_\odot$ with our SPH code until the end of the early remnant phase, and identify the mass range of CO WDs that lead to SNe Ia. Using the obtained mass range of CO WDs, we estimate the contribution of CO WD mergers to the entire population of SNe Ia in our Galaxy.

Similar parameter surveys have already been done by Dan et al. ([2012], [2014]) and Zhu et al. ([2013]). Zhu et al. ([2013]) mainly focused on the (early) remnant phase and the resolutions of their simulations are lower than those in our study. Although Dan et al. ([2012], [2014]) covered the merger phase and remnant phase, their numerical resolution is much lower than ours. We expect that SN Ia explosions occur not only in the early remnant phase but also in the dynamic merger phase. In the present work, we adopt a resolution two times higher than those in previous works (e.g., Zhu et al. [2013]). This is because the numerical resolution is one of the most important parameters for identifying the initiation of detonation in the dynamic merger phase (Pakmor et al. [2012b]). Therefore, we adopt four different resolutions and check the numerical convergence.

To investigate the possibility that carbon burning leads to an SN Ia, we check the density and temperature of SPH particles and identify carbon burning by the condition of $\tau_{\rm CC} < \tau_{\rm cool}$, where $\tau_{\rm CC}$ is the timescale of carbon burning and $\tau_{\rm cool}$ is the cooling timescale. In the dynamic merger phase, $\tau_{\rm cool}$ is the dynamic timescale of adiabatic expansion. On the other hand, in the (early) remnant phase, $\tau_{\rm cool}$ is the timescale of neutrino cooling. These are necessary but not sufficient conditions for a thermonuclear explosion. In this sense, our results would not be conclusive but are sufficiently suggestive. Since the temperature has numerical noise in our SPH simulation, we have to treat the temperature carefully. This noise comes from fluctuations of density and internal energy, which arise due to numerical resolution, finite neighboring particles, and the accuracy of time integration. We use both the raw and smoothed temperatures to estimate the noise in our SPH simulation (Dan et al. [2012]). The raw temperature is the temperature that our SPH code originally generates. The smoothed temperature is an average temperature calculated from neighboring particles, which could avoid distortion from large numerical noise (defined in Section [3.1]). In the present version of our SPH simulation, we do not include nuclear reactions because they are so sensitive to temperature noises and possibly enhance them erroneously.

This paper is organized as follows. Section [2] briefly describes our numerical methods. In Section [3], we show our results and then estimate the rate of SNe Ia coming from the DD merger systems and their contribution to the entire population of SNe Ia in our Galaxy. In Section [4], we compare our results with those from previous works and discuss the dependence of our numerical results on the resolution. Finally, we conclude the present work in Section [5].

2. METHODS

Here we present a brief summary of our numerical method. The details of the numerical method have already been described in Nakasato et al. ([2012]) and Tanikawa et al. ([2015]).

2.1. Numerical Code

SPH is the Lagrangian mesh-free particle method developed for the study of astrophysical fluid phenomena (Lucy [1977]; Gingold & Monaghan [1982]). Nowadays, it is applied in other subjects, e.g., engineering and meteorology, and has been used to make Hollywood movies. Recent good reviews of SPH codes are available, e.g., in Monaghan ([2005]) and Rosswog ([2009]). Our formulation is the one called the "vanilla ice" SPH formulation in Rosswog ([2009]). Our basic SPH equations consist of the equation of continuity, equation of motion, and energy equation for self-gravitating fluid in a Lagrangian formulation.

We use the "OcTree On OpenCL" (OTOO) code for our 3D simulations of CO WD mergers; this code was developed for various particle simulations of astrophysical fluid phenomena (Nakasato et al. [2012]). This code implements the octree method (Barnes & Hut [1986]) to calculate gravity and neighbor particles for SPH. It is optimized for multiple CPUs and GPUs in heterogeneous computational resources.

In this code, we adopt the third-order spline kernel and its derivative is modified in the same way as that proposed by Thomas & Couchman ([1992]) to avoid pairing instability. The smoothing length is determined to keep the average number of neighbors to about 75 in every step (Thacker et al. [2000]). The formulation of the artificial viscosity is basically the same as that in Monaghan ([1992]), but the viscosity coefficient is time-dependent (Morris & Monaghan [1997]). A more detailed explanation can be found in Rosswog et al. ([2000]) and Monaghan ([2005]). We also introduce the Balsara

Table 1
Summary of All Calculated Models

M_1 $(M_\odot)$	M_2 $(M_\odot)$	a_{init} $(10^9\ cm)$	T_{max} $(10^9\ K)$	$\rho(T_{max})$ $(10^6\ g\ cm^{-3})$	$T_{s,max}$ $(10^9\ K)$	$\rho(T_{s,max})$ $(10^6\ g\ cm^{-3})$	$T_{max,rem}$ $(10^9\ K)$	$\rho(T_{max,rem})$ $(10^6\ g\ cm^{-3})$	$T_{s,max,rem}$ $(10^9\ K)$	$\rho(T_{s,max,rem})$ $(10^6\ g\ cm^{-3})$
					Resolution $= 10\ k\ M_\odot^{-1}$					
1.1	1.1	1.22	2.66	6.72	1.94	7.57	1.81	2.72	1.69	3.12
1.1	1.0	1.42	1.96	3.65	1.40	9.52	1.41	1.94	1.25	2.52
1.1	0.9	1.64	1.92	3.37	1.23	6.59	1.25	3.02	1.12	2.98
1.1	0.8	1.86	1.86	1.83	1.10	4.00	1.18	2.94	1.02	2.37
1.1	0.7	2.11	1.45	0.87	1.02	3.90	1.25	1.82	0.94	2.74
1.1	0.6	2.40	1.40	1.21	0.92	3.20	1.01	2.64	0.88	2.48
1.1	0.5	2.75	1.25	1.10	0.90	1.68	0.97	1.03	0.83	2.29
1.0	1.0	1.40	2.31	4.67	1.33	4.11	1.40	3.12	1.24	3.03
1.0	0.9	1.61	1.54	3.24	0.94	3.26	1.05	2.35	0.94	2.16
1.0	0.8	1.81	1.73	2.16	0.88	2.93	0.93	2.50	0.83	2.01
1.0	0.7	2.05	1.45	1.08	0.83	0.75	0.90	2.12	0.78	2.51
1.0	0.6	2.35	1.35	1.10	0.79	1.01	0.82	2.78	0.74	2.52
1.0	0.5	2.68	1.10	0.32	0.77	1.50	0.82	3.08	0.70	1.88
0.9	0.9	1.62	1.75	2.12	0.89	1.20	0.99	2.83	0.89	1.20
0.9	0.8	1.79	1.43	1.52	0.73	2.02	0.84	2.58	0.70	1.55
0.9	0.7	2.06	1.23	1.91	0.73	1.30	0.72	2.07	0.61	1.98
0.9	0.6	2.34	1.09	0.62	0.63	0.65	0.68	1.17	0.58	1.37
0.9	0.5	2.67	1.03	0.82	0.59	0.42	0.65	2.48	0.53	1.15
0.8	0.8	1.77	1.28	2.19	0.67	1.53	0.68	1.89	0.60	1.30
0.8	0.7	2.00	1.27	1.75	0.61	1.49	0.57	0.87	0.49	1.41
0.8	0.6	2.26	1.28	0.99	0.57	0.93	0.77	1.20	0.54	1.20
0.8	0.5	2.58	0.84	0.42	0.53	1.27	0.57	0.93	0.45	0.45
0.7	0.7	1.95	0.91	1.40	0.49	1.48	0.55	0.98	0.46	1.26
0.7	0.6	2.21	1.01	1.42	0.48	0.96	0.50	1.08	0.41	1.08
0.7	0.5	2.49	0.82	0.37	0.49	0.36	0.45	0.38	0.37	0.86
0.6	0.6	2.16	0.72	1.14	0.36	0.98	0.45	0.41	0.32	0.41
0.6	0.5	2.40	0.60	0.45	0.33	0.44	0.41	1.28	0.28	1.06
0.5	0.5	2.35	0.57	1.06	0.29	0.65	0.30	0.76	0.24	0.49
					Resolution $= 50k\ M_\odot^{-1}$					
1.1	1.1	1.23	3.58	6.13	1.81	8.88	1.56	3.02	1.44	3.09
1.1	1.0	1.44	3.10	4.15	1.67	3.59	1.27	2.71	1.14	2.83
1.1	0.9	1.65	2.20	2.87	1.32	2.66	1.13	2.94	0.99	2.36
1.1	0.8	1.89	1.94	1.47	1.16	1.10	1.08	2.42	0.93	2.80
1.1	0.7	2.13	1.58	0.39	1.06	3.90	1.00	1.96	0.86	1.76
1.1	0.6	2.42	1.52	0.33	0.88	0.51	0.94	1.89	0.82	2.19
1.1	0.5	2.79	1.40	0.67	0.86	0.60	0.96	1.40	0.81	1.49
1.0	1.0	1.42	2.77	3.55	1.31	3.10	1.11	2.98	0.99	3.08
1.0	0.9	1.62	2.16	2.67	1.06	3.01	0.94	1.87	0.81	2.73
1.0	0.8	1.85	1.93	1.98	1.05	1.10	0.86	1.57	0.76	1.29
1.0	0.7	2.09	1.72	0.93	0.93	1.16	0.85	0.86	0.70	1.31
1.0	0.6	2.37	1.28	0.50	0.78	0.56	0.79	0.88	0.66	2.01
1.0	0.5	2.73	1.13	0.23	0.69	0.31	0.72	1.14	0.64	1.41
0.9	0.9	1.62	2.15	2.22	1.07	2.17	0.77	2.35	0.66	1.55
0.9	0.8	1.84	1.59	2.08	0.83	1.92	0.69	1.55	0.58	0.85
0.9	0.7	2.09	1.44	0.79	0.81	1.27	0.64	0.44	0.55	0.44
0.9	0.6	2.37	1.21	0.86	0.68	0.58	0.62	1.29	0.55	0.70
0.9	0.5	2.73	1.00	0.29	0.59	0.18	0.63	2.51	0.50	0.37
0.8	0.8	1.80	1.65	1.62	0.76	1.37	0.58	1.55	0.51	1.91
0.8	0.7	2.03	1.59	1.39	0.76	1.31	0.56	2.81	0.45	0.68
0.8	0.6	2.30	1.21	0.56	0.60	0.40	0.51	0.62	0.42	0.62
0.8	0.5	2.65	0.96	0.29	0.52	0.30	0.49	0.73	0.41	0.38
0.7	0.7	2.00	1.50	0.84	0.61	0.80	0.53	1.49	0.45	1.07
0.7	0.6	2.29	1.10	1.04	0.53	0.80	0.45	2.94	0.34	0.32
0.7	0.5	2.61	0.98	0.33	0.45	0.11	0.42	0.32	0.33	0.32
0.6	0.6	2.22	0.93	0.81	0.40	0.86	0.48	2.78	0.31	0.55
0.6	0.5	2.52	0.74	0.48	0.41	0.36	0.36	0.32	0.25	0.32
0.5	0.5	2.44	0.85	0.59	0.37	0.46	0.35	1.37	0.23	0.27

Table 1
(Continued)

M_1 $(M_\odot)$	M_2 $(M_\odot)$	a_{init} $(10^9$ cm)	T_{max} $(10^9$ K)	$\rho(T_{max})$ $(10^6$ g cm$^{-3})$	$T_{s,max}$ $(10^9$ K)	$\rho(T_{s,max})$ $(10^6$ g cm$^{-3})$	$T_{max,rem}$ $(10^9$ K)	$\rho(T_{max,rem})$ $(10^6$ g cm$^{-3})$	$T_{s,max,rem}$ $(10^9$ K)	$\rho(T_{s,max,rem})$ $(10^6$ g cm$^{-3})$
Resolution $= 100k\ M_\odot^{-1}$
1.1	1.1	1.25	3.64	5.51	1.79	3.38	1.39	2.82	1.25	2.88
1.1	1.0	1.45	3.02	6.71	1.67	3.05	1.23	2.67	1.10	3.11
1.1	0.9	1.67	2.54	4.13	1.46	4.31	1.17	2.74	1.01	1.73
1.1	0.8	1.86	2.21	1.92	1.28	1.67	1.08	2.12	0.96	2.96
1.1	0.7	2.11	1.82	1.10	1.09	0.90	0.98	2.47	0.90	1.51
1.1	0.6	2.39	1.56	0.42	0.91	0.65	0.95	1.82	0.82	1.24
1.1	0.5	2.72	1.42	1.91	0.77	0.88	0.92	0.67	0.81	0.83
1.0	1.0	1.43	3.08	4.80	1.57	4.17	0.98	3.05	0.86	2.57
1.0	0.9	1.64	2.10	3.32	1.17	2.14	0.93	1.15	0.80	1.70
1.0	0.8	1.87	1.99	2.49	1.17	1.07	0.84	0.73	0.74	0.97
1.0	0.7	2.13	1.64	1.05	0.98	0.62	0.81	0.38	0.68	0.45
1.0	0.6	2.40	1.45	1.23	0.89	0.76	0.77	0.98	0.66	1.16
1.0	0.5	2.75	1.30	0.18	0.70	0.32	0.75	0.90	0.62	0.78
0.9	0.9	1.64	2.17	3.21	0.95	2.34	0.78	2.92	0.66	2.09
0.9	0.8	1.86	1.96	1.24	1.07	1.05	0.71	1.26	0.60	0.97
0.9	0.7	2.08	1.48	1.51	0.84	0.56	0.66	0.40	0.59	0.38
0.9	0.6	2.35	1.27	0.67	0.73	0.39	0.65	0.56	0.58	0.72
0.9	0.5	2.68	1.07	0.31	0.61	0.18	0.59	0.48	0.50	0.50
0.8	0.8	1.83	1.65	2.20	0.83	3.35	0.59	2.92	0.54	1.31
0.8	0.7	2.07	1.51	0.89	0.81	0.82	0.58	0.79	0.46	0.97
0.8	0.6	2.35	1.27	0.56	0.63	0.43	0.57	0.43	0.45	0.37
0.8	0.5	2.69	1.19	0.37	0.59	0.19	0.50	2.74	0.40	0.51
0.7	0.7	2.01	1.44	1.12	0.80	1.10	0.49	0.86	0.42	0.79
0.7	0.6	2.27	1.12	0.45	0.63	0.39	0.47	0.60	0.35	0.46
0.7	0.5	2.60	0.84	0.45	0.49	0.30	0.46	0.35	0.34	0.32
0.6	0.6	2.25	1.13	0.76	0.58	0.67	0.49	2.61	0.28	0.43
0.6	0.5	2.55	0.81	0.44	0.44	0.30	0.32	2.64	0.25	0.35
0.5	0.5	2.47	0.85	0.52	0.42	0.47	0.40	1.89	0.22	0.32
Resolution $= 500k\ M_\odot^{-1}$
1.1	1.1	1.25	3.91	5.84	2.28	5.27	1.18	3.10	0.99	2.90
1.1	1.0	1.46	3.50	3.81	2.52	3.87	1.18	2.41	1.02	1.63
1.1	0.9	1.67	2.58	4.24	1.74	3.96	1.10	1.48	1.01	1.11
1.1	0.8	1.91	2.19	2.23	1.43	1.67	1.04	0.54	0.94	1.01
1.1	0.7	2.16	1.66	1.50	1.18	0.69	0.96	0.99	0.85	0.91
1.1	0.6	2.45	1.68	0.70	1.00	0.57	0.95	0.74	0.82	0.89
1.1	0.5	2.81	1.70	0.76	0.82	0.22	0.90	0.63	0.78	0.61
1.0	1.0	1.43	3.50	4.27	1.61	5.76	0.92	2.97	0.80	1.82
1.0	0.9	1.64	2.95	3.78	1.98	1.81	0.90	1.89	0.78	1.77
1.0	0.8	1.87	2.26	1.32	1.54	1.32	0.87	0.91	0.77	0.73
1.0	0.7	2.11	1.87	0.93	1.19	1.13	0.84	1.06	0.73	0.33
1.0	0.6	2.40	1.31	0.65	0.69	0.31	0.79	0.72	0.66	1.11
1.0	0.5	2.74	1.49	0.58	0.78	0.15	0.78	0.74	0.63	0.51
0.9	0.9	1.64	2.77	3.84	1.36	2.94	0.79	2.66	0.56	1.19
0.9	0.8	1.86	2.17	1.26	1.40	0.77	0.64	0.87	0.57	1.03
0.9	0.7	2.11	1.72	0.50	1.05	0.85	0.64	0.38	0.57	0.40
0.9	0.6	2.40	1.30	0.43	0.88	0.36	0.63	0.51	0.52	0.46
0.9	0.5	2.75	1.28	0.24	0.70	0.20	0.59	0.60	0.50	0.36
0.8	0.8	1.82	2.16	2.08	1.15	1.71	0.57	1.86	0.47	0.44
0.8	0.7	2.06	1.74	0.80	0.96	0.73	0.50	0.82	0.43	0.53
0.8	0.6	2.34	1.38	0.75	0.81	0.46	0.50	0.54	0.44	0.24
0.8	0.5	2.67	1.04	0.33	0.54	0.11	0.50	0.49	0.41	0.17
0.7	0.7	2.05	1.63	1.38	0.73	0.93	0.51	1.71	0.37	0.59
0.7	0.6	2.31	1.11	0.55	0.57	0.52	0.48	3.13	0.33	0.22
0.7	0.5	2.65	1.07	0.25	0.49	0.19	0.44	2.57	0.34	0.15
0.6	0.6	2.24	1.45	1.21	0.79	0.64	0.50	1.90	0.27	0.49
0.6	0.5	2.55	0.93	0.52	0.49	0.16	0.40	1.77	0.25	0.10
0.5	0.5	2.47	1.09	0.52	0.56	0.29	0.41	1.50	0.21	0.38

switch to shut off the artificial viscosity in no shock regions (Balsara 1995). We adopt a leap-frog scheme for time integration.

We use the Helmholtz equation of state (EOS) (Timmes & Swesty 2000) and assume a uniform chemical composition of 50% carbon and 50% oxygen. This chemical composition is not changed throughout the merger simulation because we do not include nuclear reactions.

2.2. Initial Setup

The initial setup of our simulations is similar to those of Rasio & Shapiro (1995) and Dan et al. (2011). We separately generate each CO WD from spherically symmetric density profiles of a perfectly degenerate star and set the temperature to 10^6 K everywhere. To reduce numerical noise in the mapping from the 1D spherically symmetric density profile to our 3D SPH density distribution, we relax the SPH particles for 20 physical seconds with velocity damping force but without the evolution of internal energy. For the damping force, we adopt

$$\frac{d\boldsymbol{v}_i}{dt} = -\frac{\boldsymbol{v}_i}{C_{\mathrm{damp}}dt}, \tag{1}$$

where $\boldsymbol{v}_i$ is the velocity of ith particle, C_{damp} is the inverse of the relaxation timescale, and we fix $C_{\mathrm{damp}} = 128.0$.

Next, we extend the distance of two CO WDs enough to avoid Roche lobe overflow (RLOF). We assume that they are on a circular orbit and their spins are synchronous with each other in orbital motion. To finish setting the initial condition, we gradually decrease the separation and relax them with the above damping force and the evolution of internal energy in a co-rotating frame. When an SPH (ith) particle of the secondary approaches close enough to the L1 point, i.e.,

$$\|\boldsymbol{r}_{\mathrm{sec},i} - \boldsymbol{r}_{\mathrm{L1}}\| < 0.2R_2, \tag{2}$$

we stop the calculation. Here $\boldsymbol{r}_{\mathrm{sec},i}$ is the position of ith particle of the secondary, $\boldsymbol{r}_{\mathrm{L1}}$ is that of the L1 point, and R_2 is the effective radius of the secondary.

Finally, we transfer the SPH particles from the co-rotating frame to a rest frame.

3. RESULTS

We summarize the results of our simulations in Table 1. Because we aim to identify the mass range of CO WDs that lead to SNe Ia, our initial models cover the entire mass range of CO WDs, i.e., from $M_{\mathrm{WD}} = 0.5$ to $1.1\ M_\odot$. We prepare binary models of 0.5, 0.6, 0.7, 0.8, 0.9, 1.0, and $1.1\ M_\odot$, and perform the simulations of mergers for all 28 mass combinations. Since we also investigate the dependence of our results on the numerical resolution, we perform the same simulations with different resolutions, which are $10k$, $50k$, $100k$, and $500k$ SPH particles per 1 solar mass (here $k \equiv 1,024$). All simulations were performed from the start of RLOF until the formation of an almost stationary remnant several hundred seconds after the secondary is completely disrupted. We divide the dynamical evolution of a merger into the following two phases: (1) the merger phase is the period during which the secondary dynamically accretes onto the primary and (2) the (early) remnant phase is from the complete disruption of the secondary to the stage where the system reaches an almost quasi-stationary state.

Figure 1 shows the density profiles in the equatorial plane for an example of our simulations whose mass combination is $1.1 + 0.9\ M_\odot$ and resolution is $500k\ M_\odot^{-1}$. The merger phase covers the first ($t = 25$ s) to fifth ($t = 135$ s) panels, and the early remnant phase corresponds to the sixth ($t = 240$ s) panel. Their morphological structures are consistent with those in previous works (e.g., Pakmor et al. 2012a).

First we check whether or not dynamical carbon burning starts in the merger phase for all simulations because it is a necessary condition for an SN Ia explosion. Then, we check steady carbon burning in the early remnant phase. If carbon burning occurs in the early remnant phase, it converts a CO WD into an ONeMg WD and the merger remnant will not become an SN Ia. Although we perform simulations with four different resolutions, we first focus on the highest resolutions ($= 500k\ M_\odot^{-1}$).

3.1. Merger Phase

Pakmor et al. (2010) first suggested that CO WD mergers lead to SNe Ia in the merger phase. They called this the (carbon-ignited) violent merger (VM) scenario. In this scenario, matter from the secondary violently accretes onto the primary and such violent accretion causes dynamical carbon burning. As a result, a detonation wave would be formed and propagate into the primary, converting its carbon–oxygen into iron group elements. Finally, the system explodes as an SN Ia. Because our simulations cannot directly resolve the initiation of detonation, we try to determine the occurrence of dynamical carbon burning in the merger phase. This condition is a necessary one for an SN Ia explosion.

For this purpose, we extract the highest temperature particle in the merger phase for all simulations. The condition for dynamical carbon burning is

$$\tau_{\mathrm{CC}} < \tau_{\mathrm{dyn}}, \tag{3}$$

where τ_{CC} is a carbon burning timescale defined by

$$\tau_{\mathrm{CC}} = \frac{C_{\mathrm{P}}T}{\epsilon_{\mathrm{CC}}}, \tag{4}$$

and τ_{dyn} is a dynamical timescale (Nomoto 1982) defined by

$$\tau_{\mathrm{dyn}} = \frac{1}{\sqrt{24\pi G\rho}}, \tag{5}$$

where C_{P} is the specific heat at constant pressure, ϵ_{CC} is the energy generation rate of carbon burning. We calculate both timescales for each particle in the merger phase and examine whether the particles satisfy Equation (3). In this work, C_{P} is derived from the Helmholtz EOS of Timmes & Swesty (2000) and ϵ_{CC} is the same as that in Dan et al. (2014), originally proposed by Blinnikov & KhoKhlov (1987). Its formulation is

$$\epsilon_{\mathrm{CC}} = \rho\, q_{\mathrm{C}}\, A_{\mathrm{T}}\, Y_{\mathrm{C}}^2\, \exp\!\left(-Q/T_{9\mathrm{a}}^{1/3} + f_{\mathrm{CC}}\right), \tag{6}$$

where $q_{\mathrm{C}} = 4.48 \times 10^{18}$ erg mol^{-1} (Blinnikov & KhoKhlov 1987), $A_{\mathrm{T}} = 8.54 \times 10^{26}T_{9\mathrm{a}}^{5/6}T_9^{-3/2}$ s^{-1} mol^{-1} cm^3, $T_9 \equiv T/10^9$ K, and $T_{9\mathrm{a}} \equiv T_9/(1 + 0.067T_9)$, $Q = 84.165$ (Fowler et al. 1975). The carbon abundance is calculated as $Y_{\mathrm{C}} = n_{\mathrm{C}}/(\rho N_{\mathrm{a}}) = 0.033$ mol g^{-1}, where n_{C} is the number density of carbon and N_{a} is Avogadro's number. A screening factor f_{CC} is ignored here because we focus on the start of dynamical carbon burning, and
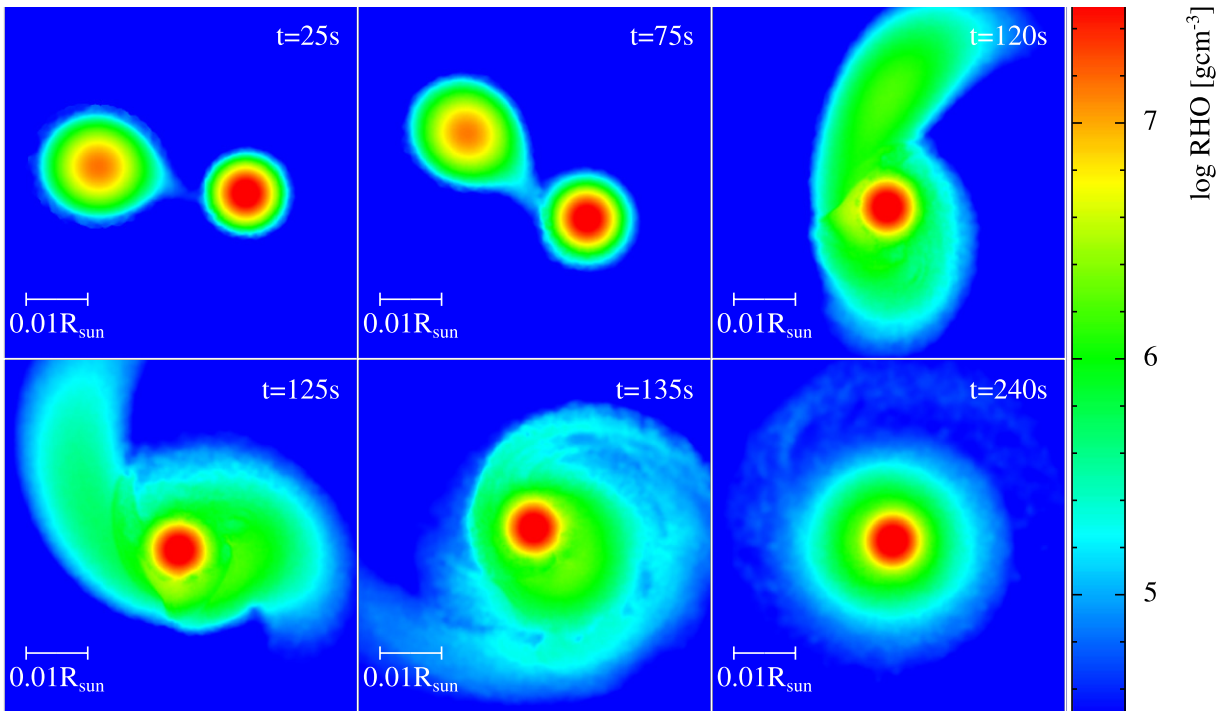
Figure 1. Density profiles in the equatorial plane for the dynamical evolution of our merger simulation. The mass combination is $1.1 + 0.9\,M_\odot$, and the resolution is $500k\,M_\odot^{-1}$. Colors indicate density on a logarithmic scale.

the factor of self-acceleration for nuclear burning described in Frank-Kamenetskii (1967) is not applied to the initiation of carbon burning.

Figure 2 shows the density and temperature of a particle with the highest temperature in the merger phase for all mass combinations (their resolutions are $500k\,M_\odot^{-1}$), similar to Figure 12 of Dan et al. (2014). The shapes and colors of symbols indicate the primary's mass and the total mass, respectively. Solid lines indicate $\tau_{CC} = \tau_{dyn}$, and dashed lines indicate $\tau_{CC} = 0.1\tau_{dyn}$. For the mass combinations above the solid line, dynamic carbon burning occurs in the merger phase. Thus, the merger of the CO WDs would lead to an SN Ia explosion.

In our SPH simulation, the physical raw temperature of each particle has numerical noise, so we adopt another definition of temperature to reduce the effect of noise, i.e., the smoothed temperature. It is defined as

$$T_{s,i} = \sum_j \frac{m_j}{\rho_j} T_j W\left(r_{ij}, h_{ij}\right), \tag{7}$$

where m_j, ρ_j, and T_j are the mass, density, and temperature of jth particle, respectively. $r_{ij} = \|\mathbf{r}_i - \mathbf{r}_j\|$, and $h_{ij} = (h_i + h_j)/2$ is the average of the smoothing lengths of the ith and the jth particles.

Figures 2(a) and (b) show the results for raw temperature and smoothed temperature thus defined, respectively. It is clear that all symbols in Figure 2(a) move to a lower place in Figure 2(b). As a result, the number of mass combinations above the solid line of $\tau_{CC} = \tau_{dyn}$ decreases. Figure 2(b) which displays the smoothed temperature shows that the mass combinations above the solid line would certainly trigger dynamic carbon burning in the merger phase.

3.2. Remnant Phase

If dynamic carbon burning does not occur in the merger phase, the merged object goes into a stationary phase, i.e., the (early) remnant phase. Figures 3(a) and (b) show the density and temperature, respectively, of a merger remnant whose mass combination and resolution are $1.1 + 0.9\,M_\odot$ and $500k\,M_\odot^{-1}$. The remnant consists of three components, i.e., a cold core, a hot envelope, and an outer disk. The structure of such a remnant has been studied in several works as mentioned in Section 1. Although there are small differences between these previous works, their results are almost consistent with each other. Our results are also consistent with these previous results.

It has long been discussed that such a hot envelope gradually accretes onto a cold core because of angular momentum loss due to some mechanism (e.g., viscosity or the magnetic field). If off-center carbon burning occurs quiescently during such an accretion phase, carbon deflagration waves propagate into the core. At last, the whole core is converted into an ONeMg WD (e.g., Saio & Nomoto 1985, 1998, 2004). In such a case, it cannot explode as an SN Ia even if its total mass exceeds M_{Ch}. Instead, it collapses to a neutron star (Nomoto & Kondo 1991). On the other hand, if off-center carbon burning does not occur, the core remains unchanged as a CO WD and the surrounding matter continues to accrete onto the core. When the core mass exceeds M_{Ch}, it explodes as an SN Ia. It is critically important to examine whether or not carbon burning starts quiescently off-center in the remnant phase.

We examine whether or not off-center carbon burning occurs in the remnant phase in the same way as that of dynamical carbon burning in the merger phase. Carbon burning quiescently occurs near the boundary between the cold core and the hot envelope if the condition for carbon
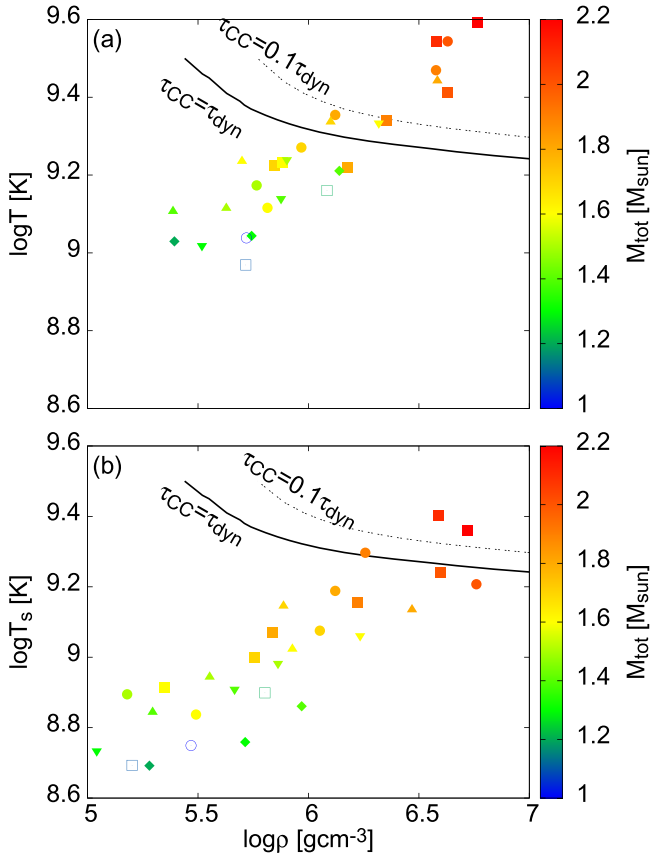
Figure 2. Density and temperature of the highest temperature particle in the merger phase for all mass combinations. Numerical resolutions of these models are $500k\,M_\odot^{-1}$. The colors of the symbols indicate the total mass of the system as indicated in the right side of the figures, and the shapes of the symbols indicate the mass of the primary. Filled squares are the $1.1\,M_\odot$ primary, filled circles $1.0\,M_\odot$, filled triangles $0.9\,M_\odot$, filled inverted triangles $0.8\,M_\odot$, filled diamonds $0.7\,M_\odot$, open squares $0.6\,M_\odot$, and open circles $0.5\,M_\odot$. Solid lines indicate $\tau_{\mathrm{CC}} = \tau_{\mathrm{dyn}}$, and dashed lines indicate $\tau_{\mathrm{CC}} = 0.1\tau_{\mathrm{dyn}}$. (a) Raw temperature of SPH particles. (b) Smoothed temperature, T_{s}, of SPH particles defined by Equation (7).

burning, i.e.,

$$\tau_{\mathrm{CC}} < \tau_\nu, \qquad (8)$$

is satisfied in the remnant phase. Here, τ_ν is a timescale of neutrino cooling and we use the description of Itoh et al. (1996) to calculate it from the density and temperature of SPH particles. We find the highest temperature particle in the remnant phase for all mass combinations and examine Equation (8). If the highest temperature particle satisfies the condition, we conclude that off-center carbon burning starts and converts the CO core into an ONeMg core. Then, the system ultimately collapses to a neutron star if the total mass exceeds M_{Ch}. On the other hand, if there are no particles that satisfy the condition and the total mass of the remnant exceeds M_{Ch}, we consider that the remnant becomes an SN Ia.

Figure 4 is the same plot as that in Figure 2, but for the remnant phase. Magenta solid lines indicate $\tau_{\mathrm{CC}} = \tau_\nu$. Figures 4(a) and (b) show results of the raw and smoothed temperatures, respectively. Off-center carbon burning occurs in the remnant phase for the mass combination models above the magenta solid line. They would ultimately collapse to a neutron star. By contrast, the models below the line would become an
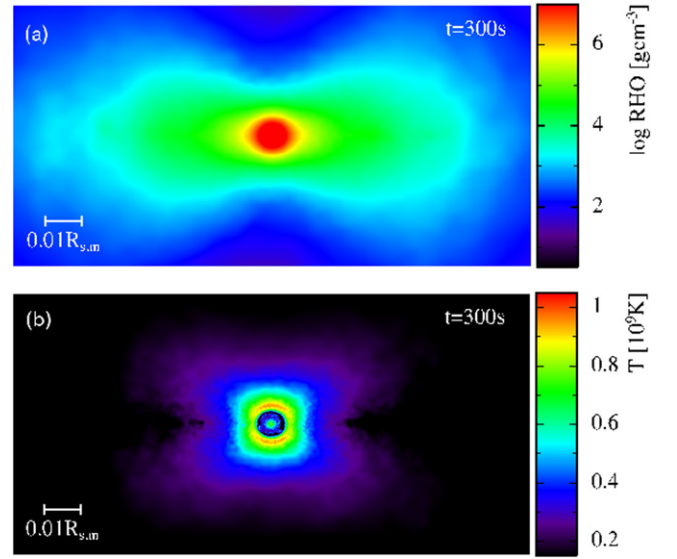
Figure 3. Structure of a merger remnant at about 200 s ($\sim 7.6\,P_{\mathrm{orb,init}}$) after the secondary is disrupted completely. Here, $P_{\mathrm{orb,init}}$ is the initial orbital period. Its mass combination is $1.1 + 0.9\,M_\odot$ and the numerical resolution is $500k\,M_\odot^{-1}$, which is the same model as in Figure 1. (a) Density profile (in a logarithmic scale of g cm^{-3}) in the x–z plane. (b) Temperature structure (in a linear scale of 10^9 K) in the x–z plane. The central part becomes slightly hot. This is caused by numerical noise and artificial viscosity, so has no physical meaning.

SN Ia if the total mass exceeds the Chandrasekhar mass, i.e., $M_1 + M_2 > M_{\mathrm{Ch}}$.

We have to follow the viscous and thermal evolution phases to obtain a definite conclusion on the off-center carbon burning. However, we stop our SPH calculation at the end of the early remnant phase because our SPH code includes no physical viscosities (e.g., magnetic viscosity). In the viscous and thermal evolution phases, the hot envelope further accretes onto the cold core and compresses itself on the cold core. When this happens, the temperature and density might further increase. As a result, carbon ignites off center even for the cases of no off-center burning in the early remnant phase. In fact, Shen et al. (2012) and Schwab et al. (2012) followed the evolution of merger remnants and showed that off-center carbon ignition starts in the viscous and thermal evolution phases in some cases. Yoon et al. (2007) performed an SPH simulation of a CO WD merger whose mass combination was $0.9 + 0.6\,M_\odot$ and further followed the evolution of the merger remnant with a 1D stellar evolution code. They found that off-center carbon burning can be avoided when the highest temperature is lower than the threshold for carbon ignition, angular momentum loss occurs with a timescale longer than that of neutrino cooling, and the mass accretion rate is $\dot{M} \leqslant 5 \times 10^{-6}$ to $10^{-5}\,M_\odot\,\mathrm{yr}^{-1}$. Our present condition for off-center carbon burning is posed only for the (early) remnant phase but not applied yet for the viscous and thermal accretion phases. In this sense, our results only for the early remnant phase are not definite answers. We leave the study of such viscous and thermal evolutions of the merger remnants to our future works.

3.3. White Dwarf Mass Combinations for SNe Ia

Now we have obtained the mass range of CO WDs, which possibly lead to SNe Ia. Using this mass range of CO WDs, we estimate their contribution to the entire population of SNe Ia
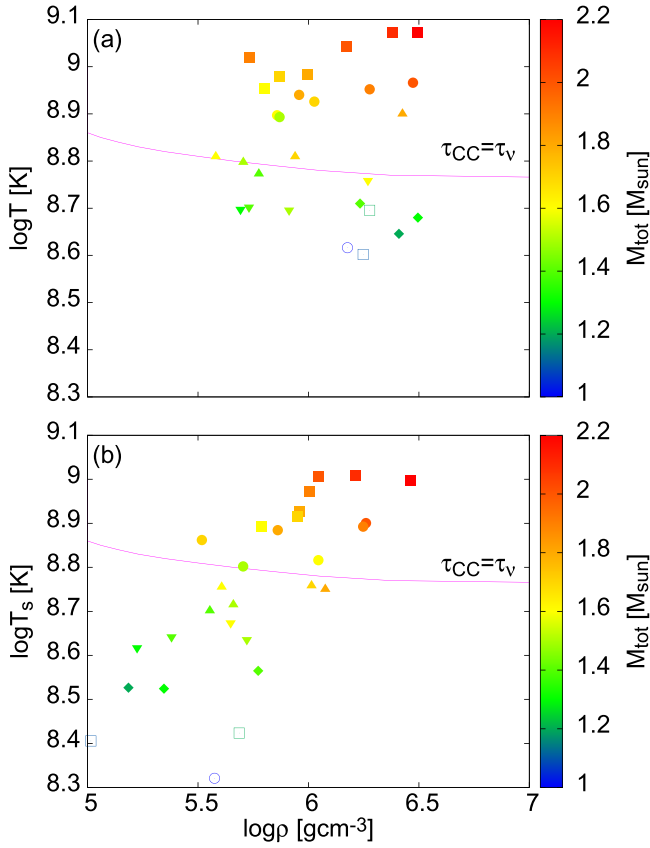
Figure 4. Same as Figure 2, but for the remnant phase. Magenta solid lines indicate $\tau_{CC} = \tau_\nu$.
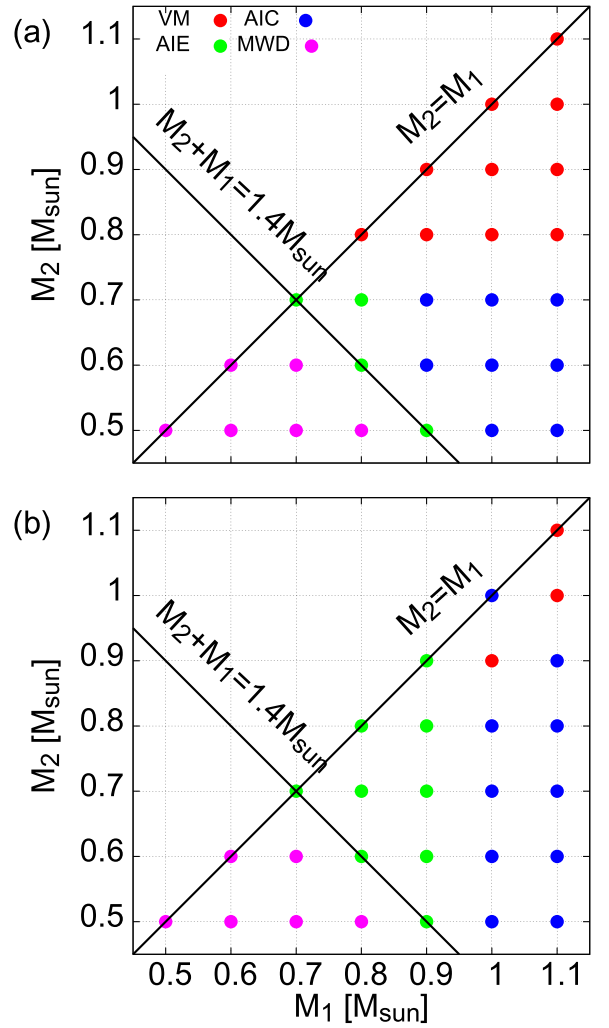

Figure 5. Outcome of our merger simulations for the (a) raw and (b) smoothed temperatures. Red symbols are the VM path, green symbols the AIE path, blue the AIC path, and magenta the MWD path. The two black lines indicate that the primary and secondary have the same mass and that the total mass equals $M_1 + M_2 = M_{Ch} \sim 1.4\, M_\odot$. Mass combinations of red and green symbols result in an SN Ia.

in our Galaxy. We consider four paths that CO WD mergers would follow. The first one is the VM path, the condition of which is that dynamic carbon burning occurs in the merger phase. The systems satisfying this condition would explode as an SN Ia immediately after merging (Pakmor et al. 2010, 2011, 2012a). When dynamical carbon burning does not occur in the merger phase, the system enters the remnant phase and the disrupted secondary surrounds the primary. If its total mass exceeds M_{Ch} and off-center carbon burning does not occur during the accretion phase, carbon burning occurs at the center of the CO WD and it would ultimately explode as an SN Ia. We regard this evolutionary path as the accretion-induced explosion (AIE) path. However, if off-center carbon burning occurs, the core of the remnant will be converted into an ONeMg WD and then collapse to a neutron star when the core mass exceeds M_{Ch}. This is the accretion-induced collapse (AIC) path (Saio & Nomoto 1985, 1998, 2004; Nomoto & Kondo 1991). When dynamic carbon burning does not occur in the merger phase and the total mass of the system does not exceed M_{Ch}, the system would form a massive CO WD. We call this evolutionary path the massive white dwarf (MWD) path.

Figure 5 shows all mass combinations of our simulations with $500k\, M_\odot^{-1}$ particles and identifies which path they take. The colors of the symbols indicate the four paths, i.e., the VM (red), AIE (green), AIC (blue), and MWD (magenta) paths. Among these four paths, the VM and AIE paths are possible paths to SNe Ia.

3.4. SN Ia Rate

We estimate the rate of SNe Ia that originate from CO WD mergers and their contribution to the entire population of SNe Ia in our Galaxy. Here we assume that all mergers of CO WDs satisfying the VM or AIE conditions can explode as SNe Ia. Strictly speaking, for the VM path, dynamic carbon burning is a necessary but insufficient condition for carbon detonation, so it is not trivial if those mergers explode as SNe Ia. We have to follow the evolution of merger remnants for a much longer time (e.g., Yoon et al. 2007) in order to identify their final fates, the AIE (exploding as an SN Ia) or AIC (collapsing to a neutron star) paths. In this sense, our estimate is just an upper limit.

The SN Ia rate depends on the Hubble types and stellar masses of galaxies. According to Li et al. (2011), in SBc-type galaxies with similar stellar masses to our Galaxy, the SN Ia rate is about $1.1 \times 10^{-13}\, yr^{-1}\, M_\odot^{-1}$. Badenes & Maoz (2012) estimated the merger rate of binary WDs in our Galaxy as $1.4 \times 10^{-13}\, yr^{-1}\, M_\odot^{-1}$. The mass distribution of binary WDs in our Galaxy is still uncertain because there are small samples
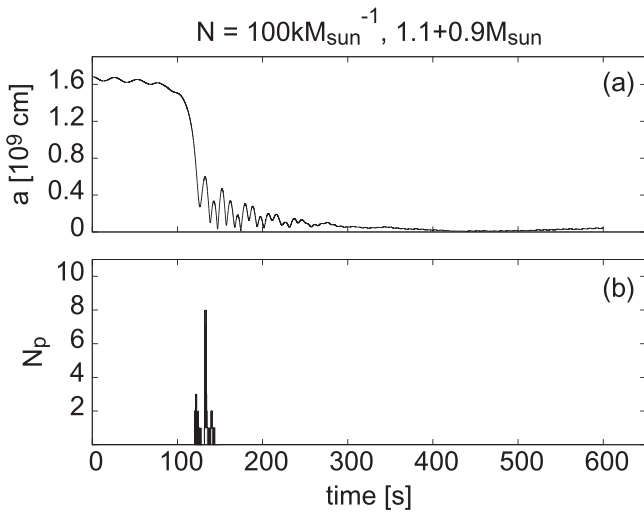
Figure 6. Time evolution of (a) the orbital separation and (b) the number of high temperature ($\geqslant 2.0 \times 10^9$ K) particles. The mass combination of WDs is $1.1 + 0.9\,M_\odot$ and the numerical resolution is $100k\,M_\odot^{-1}$.

Figure 7. Evolution of the highest temperature in each density range, $\log \rho$ (g cm^{-3}) < 5.0 (red), $5.0 < \log \rho < 5.5$ (green), $5.5 < \log \rho < 6.0$ (blue), and $6.0 < \log \rho < 6.5$ (black), for a mass combination of $0.9 + 0.6\,M_\odot$ and a resolution of $100k\,M_\odot^{-1}$.

even in our neighborhood. We assume that both the primary and the secondary follow the mass distribution of single DA WDs in our Galaxy derived from SDSS-DR7 (see, e.g., Figure 10 of Kleinman et al. 2013). Then we can calculate the rate of CO WD mergers that satisfy the condition of each scenario.

The merger rate is about $1.4 \times 10^{-15}\,\mathrm{yr}^{-1}\,M_\odot^{-1}$ ($0.14 \times 10^{-15}\,\mathrm{yr}^{-1}\,M_\odot^{-1}$) for the VM, $5.4 \times 10^{-15}\,\mathrm{yr}^{-1}\,M_\odot^{-1}$ ($8.9 \times 10^{-15}\,\mathrm{yr}^{-1}\,M_\odot^{-1}$) for the AIE path, and $6.8 \times 10^{-15}\,\mathrm{yr}^{-1}\,M_\odot^{-1}$ ($9.0 \times 10^{-15}\,\mathrm{yr}^{-1}\,M_\odot^{-1}$) for both paths if we adopt the case of raw temperature (smoothed temperature). This is only $\lesssim 9\%$ of the entire Galactic SNe Ia population. Therefore, at least in our Galaxy, DD merger systems might not be the dominate progenitors of SNe Ia.

4. DISCUSSION

4.1. Comparison with Previous Studies

We compare the present results with those from previous studies. In particular, we mainly focus on two mass combinations. One is $1.1 + 0.9\,M_\odot$ and the other is $0.9 + 0.6\,M_\odot$ because these two combinations were well studied in previous works.

4.1.1. $1.1 + 0.9\,M_\odot$

First we compare our results for $1.1 + 0.9\,M_\odot$ and $100k\,M_\odot^{-1}$ (i.e., the total number of SPH particles is about 2×10^5) with that of Pakmor et al. (2012b). Figure 6(a) shows the time evolutions of the orbital separation and Figure 6(b) shows the number of particles having temperatures higher than 2×10^9 K. Our Figure 6 should be compared with Figure 4 and Table 1 of Pakmor et al. (2012b).

It should be noted that the WDs in our model merge more quickly (about 100 s) than those in Pakmor et al. (2012b, at about 600 s) although we start our simulation with an initial condition similar to theirs. This is because our initial separation ($\sim 1.67 \times 10^9$ cm) is less than that of Pakmor et al. (2012b) ($\sim 1.93 \times 10^9$ cm). Indeed, Figures 6(a) and (b) resemble the case of their smaller initial separation. We suppose that the main reason of the difference is the relaxation method of a
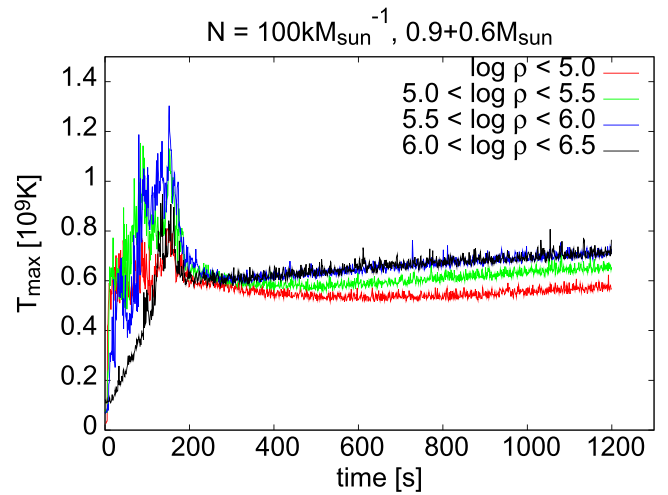
single WD. As mentioned in Section 2.2, we relax a single WD with a velocity-dependent damping force but without the evolution of internal energy. On the other hand, Pakmor et al. (2012b) changed the damping timescale (see their Equation (14)). After the relaxation method of Pakmor et al. (2012b) is applied to our models, the radii of the relaxed WDs are a few percent larger than our original ones. Therefore, their separations when the RLOF starts are larger than ours and they result in a longer merging time.

If the initial separation is smaller when the RLOF starts, the mass transfer tends to occur more violently and the secondary is completely disrupted within a few orbital periods (Dan et al. 2011). As a result, accreted matter is more strongly shock-heated and dynamic carbon burning easily occurs. Although Pakmor et al. (2012b) concluded that the initial condition is not as important for dynamic carbon burning, we should note that our highest temperatures in the merger phase could be overestimated.

4.1.2. $0.9 + 0.6\,M_\odot$

We also compare our results of $0.9 + 0.6\,M_\odot$ and $100k\,M_\odot^{-1}$ with those from the previous studies of Yoon et al. (2007), Dan et al. (2011), and Zhu et al. (2013). Since these studies have used similar resolutions (a few $\times\,10^5$ SPH particles in all), they are suitable for comparison. Figure 7 shows the time evolution of the highest temperature in each density zone. Since no dynamic carbon burning occurs (see Figure 5), we examine whether or not quiescent carbon burning occurs in the remnant phase, i.e., at $t \sim 300$ s in Figure 7. The temperature is about 6×10^8 K and this is consistent with the above three previous studies.

We compare our Figure 7 with Figure 4 in Yoon et al. (2007). For the highest temperature in the merger phase (at $t \sim 100$ s in Figure 7), their results for 1.7×10^9 K are higher than ours (1.3×10^9 K), although dynamic carbon burning does not occur in the merger phase in both our study and theirs. We suppose that the difference in the highest temperature comes from the difference in the initial condition. Dan et al. (2011) reported that the morphology of a merger remnant
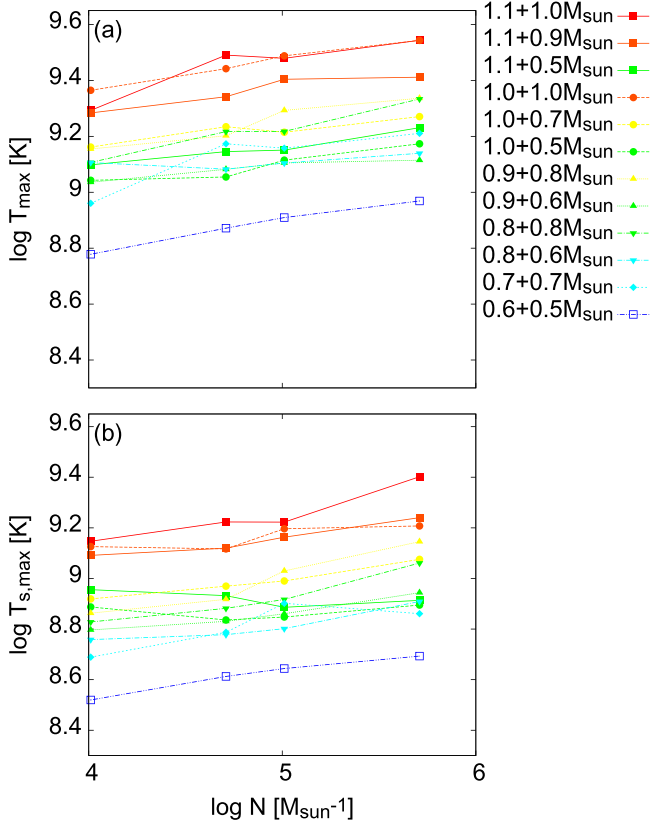
Figure 8. Dependence of the highest temperature on the numerical resolution in the merger phase for the (a) raw and (b) smoothed temperatures. The horizontal axis is the number of SPH particles per solar mass. The vertical axis is the highest temperature. The shapes and colors of the symbols have the same meanings as in Figure 2. The highest temperature tends to increase with numerical resolution.

Figure 9. Dependence of minimum τ_{CC}/τ_{dyn} ratio on the numerical resolution in the merger phase for the (a) raw and (b) smoothed temperatures. The horizontal magenta dashed lines indicate $\tau_{CC}/\tau_{dyn} = 1.0$.

could be affected by the initial condition. They found that a remnant whose initial separation is larger has a longer trailing arm than one whose initial separation is smaller (see Figure 10 of Dan et al. 2011). By contrast, we find that the highest temperature in the remnant phase is barely affected by the initial condition (see Figure 7). A similar discussion appears in Tanikawa et al. (2015).

Other factors might affect the results of our simulations. For example, Zhu et al. (2013) and Dan et al. (2014) performed merger simulations of non-spinning WDs and found that the structures of such merger remnants are different from those in mergers of synchronously spinning WDs, especially for the case of nearly equal masses. In non-spinning cases, the high temperature region is formed near the center of the merger remnant, and carbon burning might occur in that region. Since it is still uncertain whether binary WDs maintain synchronization until their mergers, our results for the AIE path might be different. The topic of synchronization is out of the scope in this paper, so we leave this to our future works.

4.2. Numerical Resolution

Pakmor et al. (2012b) concluded that the numerical resolution of a simulation is one of the most important factors for carbon burning in the merger phase because very high resolution is required to identify very small hot spots. Therefore, we examine the dependence of our results on the numerical resolution. We perform the same simulations with four different resolutions, i.e., $10k$, $50k$, $100k$, and $500k$ per 1 solar mass. The highest temperature is critical for both dynamic carbon burning and quiescent carbon burning, so we focus on the dependence of the highest temperature on the resolution.

Figures 8(a) and (b) show the dependence of the highest temperature in the merger phase on the numerical resolution for the (a) raw and (b) smoothed temperatures, respectively. The highest temperature increases with the number of SPH particles. In other words, our simulation does not converge yet and the final fates of some models could be changed from the AIC path to the VM path. Such a tendency was also reported in Pakmor et al. (2012b). In this sense, we must further increase the numerical resolution to at least more than $500k\,M_\odot^{-1}$ to definitely identify the fate of merger products. Figures 9(a) and (b) show the dependence of the minimum τ_{CC}/τ_{dyn} ratio in the merger phase on the numerical resolution for the (a) raw and (b) smoothed temperatures, respectively. The magenta dashed line indicates $\tau_{CC}/\tau_{dyn} = 1.0$. It tends to decrease as the numerical resolution increases. This trend is consistent with that of the highest temperature. For the smoothed temperature, only very massive pairs (both masses $\gtrsim 1.0\,M_\odot$) can ignite carbon dynamically.

Figures 10(a) and (b) show the highest temperature in the remnant phase for the (a) raw and (b) smoothed temperatures, respectively. Compared with the results in the merger phase (Figure 8), the highest temperature barely depends on the resolution. Especially for the smoothed temperature in Figure 10(b), it converges for almost all of the mass
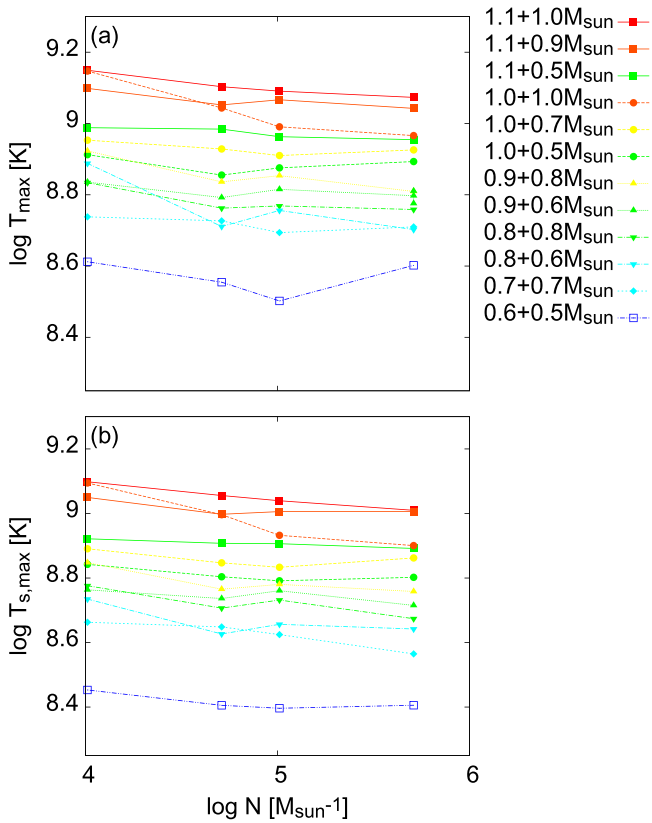
Figure 10. Same as Figure 8, but for the highest temperature in the remnant phase. The highest temperature seems to converge.

combinations. This tendency of weak dependence on the resolution has already been reported in previous studies (Raskin et al. 2012; Dan et al. 2014).

5. CONCLUSIONS

We have performed SPH simulations of CO WD mergers for the mass combinations of 0.5–1.1 $M_\odot$ from the start of the RLOF to the formation of a quasi-stationary merger remnant and examined whether carbon burning occurs either in the merger phase or the remnant phase. Using the results of SPH simulations, we have investigated the mass range of CO WDs that possibly lead to an SN Ia in the merger phase or remnant phase. We have obtained the mass range as follows. When the primary and secondary are as massive as $0.9\,M_\odot \lesssim M_{1,2} \lesssim 1.1\,M_\odot$, the binary results in an SN Ia in the merger phase. On the other hand, when the primary is $0.7\,M_\odot \lesssim M_1 \lesssim 0.9\,M_\odot$ and the total mass of the binary exceeds $1.4\,M_\odot$, they lead to an SN Ia in the remnant phase.

From the obtained mass range, we have estimated the rate of SNe Ia coming from CO WD mergers in our Galaxy. It is $6.8 \times 10^{-15}\,\mathrm{yr}^{-1}\,M_\odot^{-1}$ if we use the results of our raw temperature calculations, while it is $9.0 \times 10^{-15}\,\mathrm{yr}^{-1}\,M_\odot^{-1}$ if we use that of the smoothed temperature. These are only less than 9% of the entire SN Ia rate. Therefore, it is unlikely that the mergers of CO WDs are the main progenitors of SNe Ia.

Of course, the above estimate is not conclusive because of several uncertainties in our calculation. We have checked the dependence of the highest temperature on the numerical resolution in both the merger and the remnant phases in order to examine the numerical convergence of our simulations. We

have found that the highest temperature in the merger phase depends on the numerical resolution. It tends to increase with resolution as already reported in Pakmor et al. (2012b). In the remnant phase, the highest temperature barely depends on the numerical resolution. Therefore, it is necessary to increase the number of SPH particles up to at least $\gtrsim 500k\,M_\odot^{-1}$ to obtain a definite conclusion. Additionally, our calculations for SNe Ia in the remnant phase are not sufficient. In order to obtain a decisive conclusion, we have to follow the further evolution of the merger remnant, like Yoon et al. (2007). This will be the focus of one of our future works.

APPENDIX
SUMMARY OF CO WD MERGER SIMULATIONS

We summarize our numerical results in Table 1. The numerical values presented in the table are the primary mass, M_1, secondary mass, M_2, initial orbital separation, a_{init}, raw and smoothed maximum temperatures, T_{max} and $T_{\mathrm{s,max}}$, densities at the highest raw temperature and at the highest smoothed temperature, $\rho(T_{\mathrm{max}})$ and $\rho(T_{\mathrm{s,max}})$, in the merger phase, $T_{\mathrm{max,rem}}$, and $T_{\mathrm{s,max,rem}}$, $\rho(T_{\mathrm{max,rem}})$ and $\rho(T_{\mathrm{s,max,rem}})$ in the remnant phase.

REFERENCES

Badenes, C., & Maoz, D. 2012, ApJL, 749, L11
Balsara, D. S. 1995, JCoPh, 121, 357
Barnes, J., & Hut, P. 1986, Natur, 324, 446
Benz, W., Cameron, A. G. W., Press, W. H., & Bowers, R. L. 1990, ApJ, 348, 647
Blinnikov, S. I., & KhoKhlov, A. M. 1987, SvAL, 13, 364
Blondin, S., Prieto, J. L., Patat, F., et al. 2009, ApJ, 693, 207
Dan, M., Rosswog, S., Brüggen, M., & Podsiadlowski, P. 2014, MNRAS, 438, 14
Dan, M., Rosswog, S., Guillochon, J., & Ramirez-Ruiz, E. 2011, ApJ, 737, 89
Dan, M., Rosswog, S., Guillochon, J., & Ramirez-Ruiz, E. 2012, MNRAS, 422, 2417
Di Stefano, R., Voss, R., & Claeys, J. S. W. 2011, ApJL, 738, L1
Eggleton, P. P. 1983, ApJ, 268, 368
Fowler, W. A., Caughlan, G. R., & Zimmerman, B. A. 1975, ARA&A, 13, 69
Frank-Kamenetskii, D. 1967, Diffusion and Heat Transfer in Chemical Kinetic (Moscow: Nauka)
Fryer, C. L., Ruiter, A. J., Belczynski, K., et al. 2010, ApJ, 725, 296
Gingold, R. A., & Monaghan, J. J. 1982, JCoPh, 46, 429
Guerrero, J., Garcia-Berro, E., & Isern, J. 2004, A&A, 413, 257
Hachisu, I., Kato, M., & Nomoto, K. 1996, ApJL, 470, L97
Hachisu, I., Kato, M., & Nomoto, K. 1999a, ApJ, 522, 487
Hachisu, I., Kato, M., & Nomoto, K. 2012, ApJL, 756, L4
Hachisu, I., Kato, M., Nomoto, K., & Umeda, H. 1999b, ApJ, 519, 314

Iben, I., , Jr., & Tutukov, A. V. 1984, ApJS, 54, 335
Itoh, N., Hayashi, H., Nishikawa, A., & Kohyama, Y. 1996, ApJS, 102, 411
Ji, S., Fisher, R. T., García-Berro, E., et al. 2013, ApJ, 773, 136
Justhum, S. 2011, ApJL, 730, L34
Kashyap, R., Fisher, R., García-Berro, E., et al. 2015, ApJL, 800, L7
Kleinman, S. J., Kepler, S. O., Koester, D., et al. 2013, ApJS, 204, 5
Kobayashi, C., Tsujimoto, T., Nomoto, K., Hachisu, I., & Kato, M. 1998, ApJL, 503, L155
Li, W., Chornock, R., Filippenko, A. V., et al. 2011, MNRAS, 412, 1473
Lorén-Aguilar, P., Isern, J., & Garcia-Berro, E. 2009, A&A, 500, 1193
Lucy, L. B. 1977, AJ, 82, 1013
Maoz, D., Mannucci, F., & Nelemans, G. 2014, ARA&A, 52, 107
Moll, R., Raskin, C., Kasen, D., & Woosley, S. E. 2014, ApJ, 785, 105
Monaghan, J. J. 1992, ARA&A, 30, 543
Monaghan, J. J. 2005, RPPh, 68, 1703
Morris, J. P., & Monaghan, J. J. 1997, JCoPh, 136, 41
Nakasato, N., Ogiya, G., Miki, Y., Mori, M., & Nomoto, K. 2012, arXiv:1206.1199
Nomoto, K. 1982, ApJ, 257, 780
Nomoto, K., & Kondo, Y. 1991, ApJL, 367, L19
Pakmor, R., Edelmann, P., Röpke, F. K., & Hillebrandt, W. 2012b, MNRAS, 424, 2222
Pakmor, R., Hachinger, S., Röpke, F. K., & Hillebrandt, W. 2011, A&A, 528, A117
Pakmor, R., Kromer, M., Röpke, F. K., et al. 2010, Natur, 463, 61
Pakmor, R., Kromer, M., Taubenberger, S., et al. 2012a, ApJL, 747, L10
Patat, F., Chandra, P., Chevalier, R., et al. 2007, Sci, 317, 924
Perlmutter, S., Aldering, G., Goldhaber, G., et al. 1999, ApJ, 517, 565
Price, D. J. 2007, PASA, 24, 159
Rasio, F. A., & Shapiro, S. L. 1995, ApJ, 438, 887
Raskin, C., & Kasen, D. 2013, ApJ, 772, 1

Raskin, C., Kasen, D., Moll, R., Schwab, J., & Woosley, S. E. 2014, ApJ, 788, 75
Raskin, C., Scannapieco, E., Fryer, C., Rockefeller, G., & Timmes, F. X. 2012, ApJ, 746, 62
Riess, A. G., Fillipenko, A. V., Challis, P., et al. 1998, AJ, 116, 1009
Rosswog, S. 2009, NewAR, 53, 78
Rosswog, S., Davies, M. B., Thielemann, F. K., & Piran, T. 2000, A&A, 360, 171
Saio, H., & Nomoto, K. 1985, A&A, 150, L21
Saio, H., & Nomoto, K. 1998, ApJ, 500, 388
Saio, H., & Nomoto, K. 2004, ApJ, 615, 444
Schaefer, B., & Pagnotta, A. 2012, Natur, 481, 164
Schwab, J., Shen, K. J., Quataert, E., Dan, M., & Rosswog, S. 2012, MNRAS, 427, 190
Segretain, L., Chabrier, G., & Mochkovitch, R. 1997, ApJ, 481, 355
Shen, K. J., Bildsten, L., Kasen, D., & Quataert, E. 2012, ApJ, 748, 35
Shen, K. J., Guillochon, J., & Foley, R. 2013, ApJL, 770, L35
Simon, J. D., Gal-Yam, A., Gnat, O., et al. 2009, ApJ, 702, 1157
Soker, N., Kashi, A., García-Bero, E., Torres, S., & Camacho, J. 2013, MNRAS, 431, 1541
Sternberg, A., Gal-Yam, A., Simon, J. D., et al. 2011, Sci, 333, 856
Tanikawa, A., Nakasato, N., Sato, Y., et al. 2015, ApJ, in press (arXiv:1504.06035)
Thacker, R. J., Tittley, E. R., Pearce, F. R., Couchman, H. M. P., & Thomas, P. A. 2000, MNRAS, 319, 619
Thomas, P. A., & Couchman, H. M. P. 1992, MNRAS, 257, 11
Timmes, F. X., & Swesty, F. D. 2000, ApJS, 126, 501
Webbink, R. F. 1984, ApJ, 277, 355
Whelan, J., & Iben, I., Jr. 1973, ApJ, 186, 1007
Yoon, S. C., Podsiadlowski, P., & Rosswog, S. 2007, MNRAS, 380, 933
Zhu, C., Chang, P., van Kerkwijk, M. H., & Wadsley, J. 2013, ApJ, 767, 164